GAUSSIAN NOISE (GN) MODEL EXPERIMENTAL VALIDATION ON SHORT SPAN OPTICAL FIBER TRANSMISSION SYSTEM

by

Farida Purnama Sari

A Thesis Submitted to the Faculty of the

COLLEGE OF OPTICAL SCIENCES

In Partial Fulfillment of the Requirements

For the Degree of

MASTER OF SCIENCE

In the Graduate College

THE UNIVERSITY OF ARIZONA

2019

THE UNIVERSITY OF ARIZONA
GRADUATE COLLEGE

As members of the Master's Committee, we certify that we have read the thesis prepared by Farida Purnama Sari, titled *Gaussian Noise (GN) Model Experimental Validation on Short Span Optical Fiber Transmission* and recommend that it be accepted as fulfilling the dissertation requirement for the Master's Degree.

Daniel C. Kilper Date: 12/5/19

Khanh Q. Kieu Date: 12/05/19

Ivan B. Djordjevic Date: 12/05/19

Final approval and acceptance of this thesis is contingent upon the candidate's submission of the final copies of the thesis to the Graduate College.

I hereby certify that I have read this thesis prepared under my direction and recommend that it be accepted as fulfilling the Master's requirement.

Daniel C. Kilper Date: 12/5/19
Master's Thesis Committee Chair
James C. Wyant College of Optical Sciences

Table of Contents

List of Figures

1. Abstract

Nonlinear signal impairments are among the most critical phenomena in long-haul optical communication system transmission. Therefore, it is important to include a nonlinear impairment model in the Quality of Transmission (QoT) prediction algorithms. While many models to account for the fiber nonlinearities in optical fiber transmission have been proposed, the practical value of a model is also a consideration for implementation and calculation time is a particularly important factor.

The Gaussian noise (GN) model accounts for the nonlinear signal impairment impact using a simple closed-form formula, reducing the complexity of the computation process and computation time. With reasonable accuracy, the GN model has become a powerful tool that has been implemented in many physical environment based QoT predictions [7][10], including a Python implementation that is being developed by an industry group, known as GNPy[10].

GN model performance in predicting long-haul transmission effects has been experimentally validated by many researchers on various types of networks. In many emerging networks, however, it is common to have non-homogeneous links and short span lengths, such as in a metro network, which are not accounted for in the original GN model. Furthermore, many optical networking lab experiments do not allow for recirculating loop methods and therefore long distance, many hop experiments are problematic. Since nonlinear fiber effects are power dependent, long distance transmission can be emulated by artificially increasing the signal power. In such scenarios, the conditions that allow for a Gaussian noise statistics approach might not be satisfied and the accuracy of the GN model may be compromised. Therefore, the performance of

the GN model is tested on a coherent optical communication system testbed using 1 and 2 spans for high signal powers.

In this experiment, it is shown that the calculated P_{NLI} using GN model is overestimated results in the deviation of the calculated gOSNR from the measured gOSNR. The P_{NLI} is also measured using several other models to increase its accuracy, such as using GN model with correction factor, model for DM transmission, and gnpy. However, these models only show slight improvement to the gOSNR calculation accuracy. The deviation of the calculated gOSNR is possibly due to the lack of signal dispersion in the first few spans results in the failing gaussianization of the nonlinear signal. Also, the strong SPM and XPM noise combined with the interaction of the nonlinear noise with the ASE produced by the last amplifier introducing a strong nonlinear phase noise and contribute to the significant error in GN model prediction.

The main contribution of this thesis is as an early study of the GN model to estimate performance and simulate transmission using short spans, which is common in metro networks. Also, by exploiting the power and span dependency of nonlinear noise power, the nonlinear effect in multi-hop span transmission can be emulated using a single span. This will be beneficial in lab setups that have limited resources or do not allow for recirculating loop experiments.

2. Introduction

The Internet capacity demand is projected to increase exponentially every year [1], especially with the upcoming implementation of Internet of Things (IoT) and 5G that requires such high speed and data volume to be delivered to the customer.

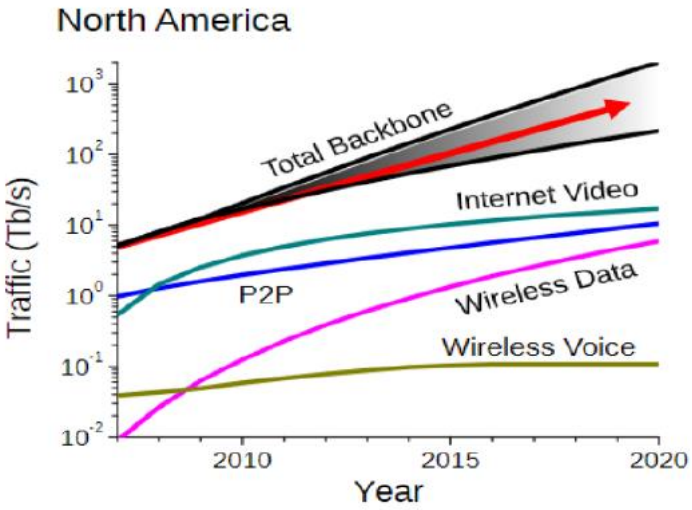

Figure 2.1. Internet Capacity Demand Projection [1]

To accommodate this Internet demand in the future, fiber optics has always been one of the most promising options for delivering reliable high-speed Internet access with good quality of service (QoS), either in the backbone or metro/access network. However, in optical transmission communication systems, there are some degrading signal impairments that are inevitable. One is the Amplified Spontaneous Emission (ASE) noise as a result of the signal amplification process in Erbium-doped fiber amplifiers (EDFA) and another is the noise due to the nonlinear fiber response to optical power. These signal impairments due to the nonlinear fiber response becomes more significant as the optical power, transmission length, transmission rates, and the number of wavelength signals in the fiber are increased. High optical power levels in a transmission system can cause the non-linearity that is induced by the change of the material refractive index in

proportion to the signal electric field intensity or also known as Kerr-Effect [3]. As the length of the transmission increases, this effect is accumulated creating significant additional noise in the system that must be addressed to maintain the quality of the transmission.

Other critical impairments that are also occurring in long-haul transmission is the fiber group velocity dispersion. Various compensation methods were developed to deal with this effect, such as deploying dispersion-compensating fiber (DCF). The type of transmission where the dispersion compensating fiber method is applied is known as the Dispersion-Managed Transmission (DMT). In DMT, the length of transmission can be extended without much degradation in quality, particularly for on-off keyed modulation formats [2]. However, some studies showed that uncompensated transmission (UT) links yield better performance for signals using advanced modulation formats such as quadrature amplitude modulation [5]. Furthermore, various studies showed that some perturbative models could give an accurate prediction of the fiber nonlinearity impairments in UT links, that did not perform well in links with dispersion management (DM) [5]. Fiber nonlinear effects are commonly modeled by solving the Nonlinear Schrodinger Equation (NLSE), for example by using the Split Step Fourier Method (SSFM), which is numerically intensive and not practical for online or real time performance estimation.

In Gaussian noise (GN) model provides another approach in which the signal distortion due to nonlinear fiber effects is assumed to have additive Gaussian noise characteristics and can be added incoherently, thus reducing the complexity of the computational process significantly. Even though many assumptions are made in applying this model, researchers have found that it works well in a surprisingly wide range of network configurations, such as networks with a wide range of modulation formats [5]. However, to increase the accuracy of the GN model, some improved models are also being proposed such as, the Enhanced Gaussian Noise (EGN) model

[4]. EGN, which take away the Gaussianity assumption from one of the NLI noise components. This approach shows great improvement in the accuracy of the model although it is more complex compared the GN model.

Also, it is possible that a network topology consists of different regions with unique characteristics such as fiber type or amplifier type, hence creating non-homogeneous links. With the GN model, this problem can be overcome by inspecting each fiber span individually. While the noise 'Gaussianization' assumption is well-established in many studies for long haul transmission [5][6], the Gaussianity of the non-linear noise distribution in a single span WDM network is not well studied. This case may apply for metro networks or edge cloud networks that normally consist of 1 to as many as 20-30 short distance spans. In many cases, the total accumulated dispersion over these distances may not be sufficient to achieve the signal characteristics of a UT link for which the GN model works well. At the same time, high optical power transmission is desirable in order to increase the signal constellation size and transmit larger amounts of information per symbol. At high powers, the fiber nonlinear effects will again become important. Furthermore, single span transmission with high signal power is often used in lab experiments to emulate the nonlinear effects of long-distance transmission. Therefore, it is of interest to study the single, short span case in the high signal power limit to establish the conditions for accurate emulation of longer transmission distances.

In future networks in which the optical systems are expected to be more scalable and flexible it is anticipated that dynamic bandwidth allocation and wavelength assignment will be used. For such optical switching functionality, it is important to be able to predict the QoT of the system before a desired wavelength or modulation scheme is assigned. As a result, many researchers have recently focused on developing more accurate and rapid QoT prediction methods

[7][8][9]. The GN model is mostly used in physical environment simulation for QoT, such as gnpy. This open source performance estimator has been tested over various commercial testbeds and shows good accuracy by in using the GN model to account for nonlinear impairments in its simulation [9].

In this work, the performance of the GN model at predicting the signal quality in a link that consists of 2 spans each 25 km in length will be experimentally studied. The optical power launched into each transmission span will be varied over a wide range in order to capture the nonlinear effects at these short distances. Combining the GN model nonlinear noise estimation with the measured optical signal-to-noise ratio (OSNR) will be used to determine the generalized OSNR, which is a common metric of QoT evaluation. The results will also be used to evaluate the potential for emulating longer distance transmission with using a small number of spans.

3. Nonlinear Impairments in Coherent Optical Systems

The research in coherent optical communications has started in early 1970 and was studied extensively in the early 1980's due to interest in receiver sensitivity advantages and the potential to elongate the unrepeated transmission distance. The difficulties in performing carrier recovery at high speed in the face of optical polarization and nonlinear effects resulted in coherent systems being abandoned for over two decades. Increasing bandwidth demand driving a need for greater spectral efficiency in optical network transmission and advances in high speed digital signal processing have made optical coherent systems gain renewed popularity to the point that today they are exclusively used in new long haul deployments. The demonstration of digital carrier phase estimation in 2005 opened up the possibility of using various spectrally efficient modulation techniques such as M-ary Phase Shift Keying (PSK) and quadrature amplitude modulation (QAM) [11].

As opposed to the Intensity Modulation/Direct Detection (IM/DD) where information bits are modulated into the intensity of the laser source, in coherent communication systems, information bits can be modulated in the amplitude, phase, or both on the laser source using an external modulator and detected coherently in the receiver.

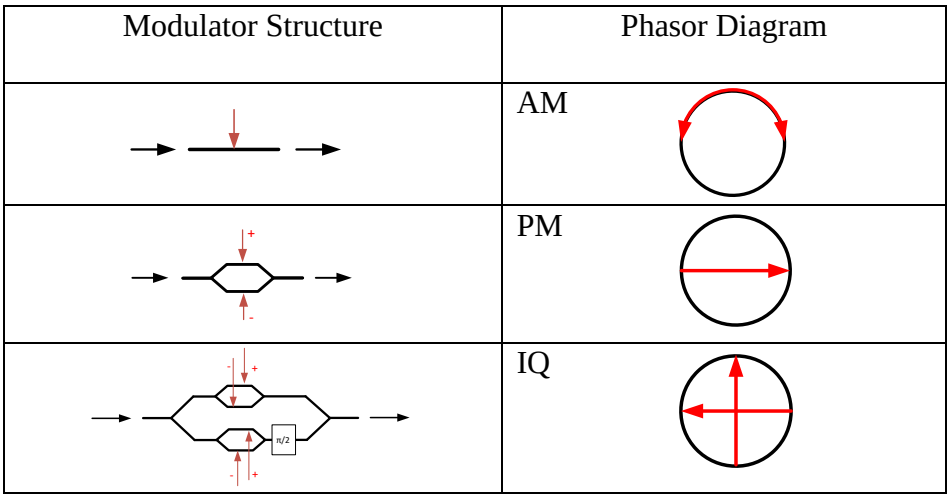

Figure 3.1. Comparison of the device structure between intensity modulation, phase modulation, amplitude modulation, and IQ modulation [11].

Figure 3.1 above shows how different types of modulation can be performed using Mach-Zhender modulators in push-pull operation mode. Using an IQ modulator, the information signal can be represented in any combination of amplitude and phase as we can see in the figure below.

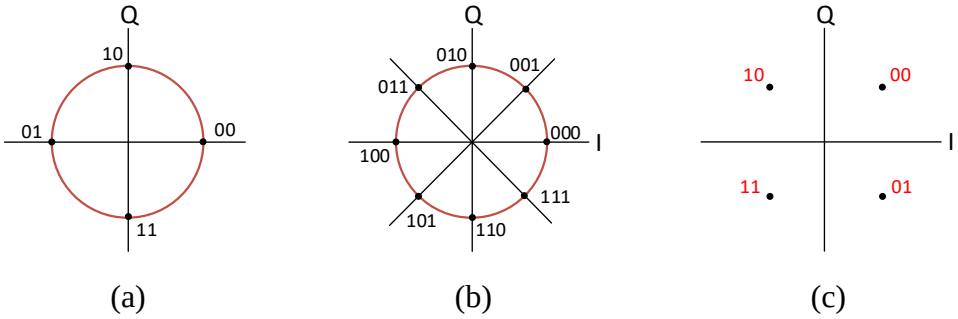

Figure 3.2. Constellation diagrams of (a) 4-PSK (b) 8-PSK (c) 4 -QAM

For a polarization diverse modulation scheme, two IQ modulators can be used to modulate each polarization and both signals later can be combined using a polarization beam combiner (PBC). Or instead using one IQ modulator and split the signal at the output using a polarization beam splitter (PBS). One of the signals goes to an RF delay and controlled by a polarization controller before the signal is combined back using a PBC.

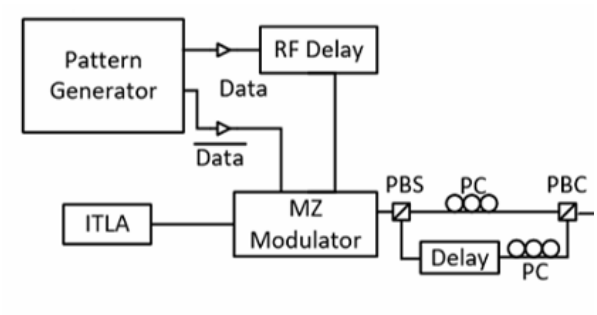

Figure 3.3 Configuration of dual polarization IQ modulation system

Figure 3.4 IQ Modulator consists of two parallel mach-zender modulator

3.1. Optical Coherent Receiver

On the receiver side, the signal is detected coherently using an optical homodyne, intradyne, or heterodyne detector. The basic principle of coherent detection is to take the product of the transmission signal carrying data information and the continuous wave (CW) local oscillator. The electric field of the optical signal coming from the transmitter is:

$$E_s(t) = A_s(t)\exp(-i\omega_s t) \tag{3.1}$$

where $A_s(t)$ is the complex amplitude, including the amplitude and phase modulation, and ω_s is the angular frequency of the signal, the wave from the LO will have a similar form, that is:

$$E_{LO}(t) = A_{LO}(t)\exp(-i\omega_{LO} t) \tag{3.2}$$

where $A_{LO}(t)$ is the complex amplitude and ω_{LO} is the angular frequency of the LO. The electrical amplitude for both the signal wave and the LO is related to the power by:

$$P_s = \frac{|A_s|^2}{2} \tag{3.3}$$

and

$$P_{LO} = \frac{|A_{LO}|^2}{2} \tag{3.4}$$

In balanced detection, a 3db coupler is used to introduce a 180^o phase shift to either the signal or LO field to suppress the DC component and maximize the signal photocurrent.

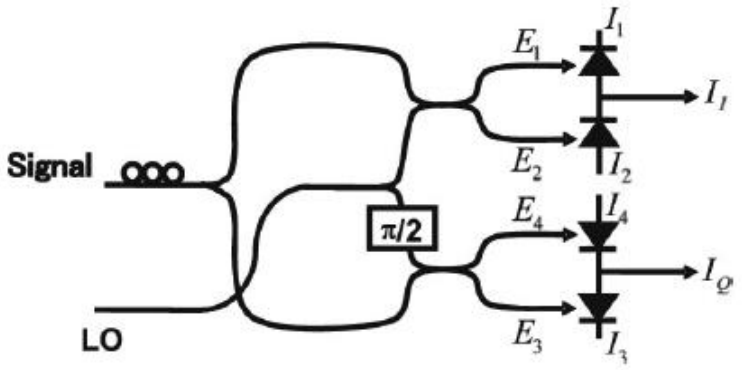

Figure 3.5 Configuration of coherent receiver with balanced detection [11].

When both signal and LO are co-polarized, the detected electric field in each photodiode is described as:

$$E_1 = \frac{1}{\sqrt{2}}(E_s + E_{LO}) \quad \text{and} \quad E_2 = \frac{1}{\sqrt{2}}(E_s - E_{LO}) \tag{3.5, 3.6}$$

while the output photocurrents are described as:

$$I_1(t) = R\left[Re\left\{\frac{A_s(t)\exp(i\omega_s t) + A_{LO}(t)\exp(j\omega_{LO}t)}{\sqrt{2}}\right\}\right]^{ms}$$

$$= \frac{R}{2}\left[P_s(t) + P_{LO} + 2\sqrt{P_s(t)P_{LO}}cos\{\omega_{IF}t + \theta_{sig}(t) - \theta_{LO}(t)\}\right] \tag{3.7}$$

and

$$I_2(t) = R\left[Re\left\{\frac{A_s(t)\exp(i\omega_s t) - A_{LO}(t)\exp(j\omega_{LO}t)}{\sqrt{2}}\right\}\right]^{ms}$$

$$= \frac{R}{2}\left[P_s(t) + P_{LO} - 2\sqrt{P_s(t)P_{LO}}cos\{\omega_{IF}t + \theta_{sig}(t) - \theta_{LO}(t)\}\right] \tag{3.8}$$

where $\omega_{IF} = |\omega_s - \omega_{LO}|$, θ_{sig} and θ_{LO} are defined as the phase of the transmitted signal and the LO respectively. R is the responsivity of the photodiode, described as:

$$R = \frac{e\eta}{\hbar\omega_s} \tag{3.9}$$

where e is the electron charge, $\hbar$ is the Planck's constant, and η is the quantum efficiency of the photodiode. Therefore, the signal detected in the photodiode is then:

$$I(t) = I_1(t) - I_2(t) = 2R\sqrt{P_s(t)P_{LO}}cos\{\omega_{IF}t + \theta_{sig}(t) - \theta_{LO}(t)\} \tag{3.10}$$

3.1.1 Heterodyne Detection

Heterodyne detection was originally developed for radio frequency (RF) and microwave signals and studied extensively in the 1960's after the initiation of the first laser [12]. The main principle of this technique is to mix the signal with another signal from a local oscillator to produce a lower frequency signal called Intermediate Frequency (IF)

The signal phase is given as $\theta_{sig}(t) = \theta_s(t) + \theta_{sn}(t)$, where $\theta_s(t)$ and $\theta_{sn}(t)$, is the phase modulation and the phase noise, respectively. The output intensity is then given as:

$$I(t) = 2R\sqrt{P_s(t)P_{LO}}cos\{\omega_{IF}t + \theta_{sig}(t) - \theta_{LO}(t)\} \tag{3.11}$$

where the complex amplitude is:

$$I_c(t) = 2R\sqrt{P_s(t)P_{LO}}\exp i\{\theta_s(t) + \theta_n(t)\} \tag{3.12}$$

and $\theta_n(t)$ is the total phase noise given as:

$$\theta_n(t) = \theta_{sn}(t) - \theta_{LO}(t) \tag{3.13}$$

To detect the heterodyne signal synchronously, an electrical phase locked loop (PLL) can be used to detect the phase of the symbol. The PLL will estimate the phase noise $\theta_n(t)$ and decode the symbol despite the variation of phase noise with time.

3.1.2 Homodyne Detection

Homodyne detection refers to the condition where the LO in the receiver has the same frequency as the frequency of the received signal ($\omega_{IF} = 0$). Therefore, the received current at the photodiode becomes:

$$I(t) = 2R\sqrt{P_s(t)P_{LO}}cos\{\theta_{sig}(t) - \theta_{LO}(t)\} \tag{3.14}$$

In the earlier development, tracking the phase and amplitude of the signal is realized by optical phase locked loop (OPLL). However, adding an OPLL increases the complexity of the system. Also, according to Eq. (3.14) above, the photodetector can only detect the cosine function which represents the in-phase component. To extract the quadrature component, another LO with 90^o phase shift is needed.

3.1.3 Intradyne Detection

By providing another LO that has 90^o shift at the detector to provide phase diversity, the detector will be able to detect the complex component as opposed to the real component that is detected by the conventional homodyne detection.

Using the configuration from Figure 3.1.1, four outputs are obtained:

$$E_1 = \frac{1}{2}(E_s + E_{LO}) \tag{3.15}$$

$$E_2 = \frac{1}{2}(E_s - E_{LO}) \tag{3.16}$$

$$E_3 = \frac{1}{2}(E_s + iE_{LO}) \tag{3.17}$$

$$E_4 = \frac{1}{2}(E_s - iE_{LO}) \tag{3.18}$$

with the output photocurrents from the balanced photodiodes:

$$I_I(t) = I_{I1}(t) - I_{I2}(t) = R\sqrt{P_s P_{LO}}\cos\{\theta_{sig}(t) - \theta_{LO}(t)\} \tag{3.19}$$

$$I_Q(t) = I_{Q1}(t) - I_{Q2}(t) = R\sqrt{P_s P_{LO}}\sin\{\theta_{sig}(t) - \theta_{LO}(t)\} \tag{3.20}$$

Therefore, the complex amplitude:

$$I_c(t) = I_I(t) + iI_Q(t) = R\sqrt{P_s P_{LO}}\exp\left[i\{\theta_s(t) + \theta_n(t)\}\right] \tag{3.21}$$

This phase diversity detection technique is also known as phase-diversity homodyne receiver or intradyne receiver. This approach has an important advantage in the IF condition because in an intradyne receiver ω_{IF} does not necessarily have to be zero, instead it only needs to satisfy $|\omega_{IF}| < 2T$, where 2T is the bandwidth of the receiver electronics.

3.2 Nonlinear Fiber Transmission Impairments

In long haul fiber optic transmission, non-linear effects are inevitable as the transmission length increases. The most important non-linear effect is the Kerr Effect which manifests as Self-Phase Modulation (SPM) and Cross-Phase Modulation (XPM). Four wave mixing (FWM), Raman scattering and Brillouin scattering can also be significant under certain conditions. In this section, some of the significant nonlinear impairments in fiber optics transmission will be discussed.

3.2.1. Kerr-Effect

The refractive index of many materials is related to electric field by the expression below:

$$n = n_0 + \bar{n}_2 \langle \boldsymbol{E}^2 \rangle \tag{3.22}$$

where n_0 is the weak-field refractive index and $\bar{n}_2$ is called the second-order index of refraction that gives the rate of increase in the overall refractive index due to the change of electric field with the brackets on $\boldsymbol{E}^2$ representing the time average.

Therefore, if light with optical field:

$$\boldsymbol{E} = E(w)e^{-i\omega t} + c.c \tag{3.23}$$

$$\langle \boldsymbol{E}(t)^2 \rangle = 2\boldsymbol{E}(\omega)\boldsymbol{E}(\omega)^* = 2|E(\omega)|^2 \tag{3.24}$$

hits a material with refractive index as given in the Eq. (3.22) above, the refractive index of that material will change into:

$$n = n_0 + 2\bar{n}_2 |E(\omega)|^2 \tag{3.25}$$

The direct expression to the optical intensity is given as:

$$n = n_0 + n_2 I \tag{3.26}$$

This change of refractive index is called the optical Kerr-Effect. However, at extremely high intensity, the change of the refractive index will not increase further due to saturation effects.

The Kerr-Effect can occur in multiple materials, such as crystal, glass, and gases. However, the interaction of light with a nonlinear medium can modify the polarization of the material system that can be described as below:

$$P^{NL}(\omega) = 3\varepsilon_0\chi^{(3)}(\omega)|E(\omega)|^2E(\omega) \tag{3.27}$$

Assuming the light is linearly polarized, the total polarization of the material system is then given as:

$$P^{TOT}(\omega) = \varepsilon_0\chi^{(1)}E(\omega) + 3\varepsilon_0\chi^{(3)}|E(\omega)|^2E(\omega) \equiv \varepsilon_0\chi_{eff}E(\omega) \tag{3.28}$$

where the effective susceptibility is defined as:

$$\chi_{eff} = \chi^{(1)} + 3\chi^{(3)}|E(\omega)|^2 \tag{3.29}$$

The nonlinear susceptibility, $\chi^{(3)}$, is related to the nonlinear refractive index via the following relation:

$$n^2 = 1 + \chi_{eff} \tag{3.30}$$

By putting in Eq. (3.25) and Eq. (3.29) into the above expression, we obtain the expression below:

$$[n_0 + 2\bar{n}_2|E(\omega)|^2]^2 = 1 + \chi^{(1)} + 3\chi^{(3)}|E(\omega)|^2 \tag{3.31}$$

The above expression then can be expanded to:

$$n_0^2 + 4n_0\bar{n}_2|E(\omega)|^2 = \left(1 + \chi^{(1)}\right) + \left[3\chi^{(3)}|E(\omega)|^2\right] \tag{3.31}$$

showing the linear and nonlinear refractive index related to the linear and nonlinear susceptibilities by the expression:

$$n_0 = \left(1 + \chi^{(1)}\right)^{\frac{1}{2}} \quad (3.32) \qquad \text{and} \qquad \bar{n}_2 = \frac{3\chi^{(3)}}{4n_0} \quad (3.33)$$

The refractive index changes induced by this Kerr-Effect as shown above cause phase changes in different parts of the optical pulse to travel at different speed causing new frequencies to appear in the transmission. The Kerr-Effect that induces phase change of a signal due to its own intensity variation is known as self-phase modulation (SPM) while the Kerr-Effect that induces phase change of a signal in another channel is known as cross-phase modulation (XPM). Both effects will be discussed further in the sections below.

3.2.2. Nonlinear Schrödinger Equation and Split-Step Fourier Method

With the addition of nonlinear polarization, $\boldsymbol{P^{NL}}$, the wave equation in the medium can be expressed as below:

$$\nabla^2 \boldsymbol{E} = \mu_0 \frac{\partial^2 \boldsymbol{D}}{\partial t^2} \quad (3.34)$$

$$\boldsymbol{D} = \varepsilon \boldsymbol{E} + P^{NL} \quad (3.35)$$

P^{NL} is assumed to be small and is treated as the perturbation from the linear polarization. With the assumption that the polarization is maintained along the transmission, the scalar approach is then valid. Next, the optical field is assumed to be sufficiently small compared to the center angular frequency, ω_0, or also known as the slowly varying envelope approximation (SVEA). In this approximation, the rapidly varying part of the electric field, $\boldsymbol{E}(\boldsymbol{r}, t)$, is separated from the slowly varying envelope as:

$$\boldsymbol{E}(\boldsymbol{r}, t) = \frac{1}{2}\boldsymbol{u}_x[E(\boldsymbol{r}, t)\exp(-i\omega_0) + cc]$$

(3.36)

where $\boldsymbol{u}_x$ is the polarization unit vector of the light is assumed to be linearly polarized along the x-axis. When we add the optical loss or gain to the refractive-index change caused by the Kerr Effect, we obtained the expression below:

$$\boldsymbol{D} = \varepsilon \boldsymbol{E} + \boldsymbol{P^{NL}} = \varepsilon_0 (n + n_2 |E|^2 - i\frac{\alpha}{k})^2 \boldsymbol{E}$$

(3.37)

where α is the attenuation coefficient and $k = \frac{\omega_0}{c}$. Assuming the nonlinear polarization and attenuation coefficient are small, Eq. (3.37) can be expressed as separated components:

$$\varepsilon \boldsymbol{E} = \varepsilon_0 \left(n^2 - i2n\frac{\alpha}{k}\right) \boldsymbol{E}$$

(3.38)

$$P^{NL} = 2\varepsilon_0 n \bar{n}_2 |E|^2 \boldsymbol{E}$$

(3.39)

The envelope function of the electric field is then expressed as the product of the transverse field distribution $R\ (r, \theta)$, and the axial amplitude variation $A(z,t)\exp(-i\beta_0 z)$:

$$E(r,t) = R\ (r, \theta) A(z,t) \exp(-i\beta_0 z)$$

(3.40)

where β_0 denotes the propagation constant in the absence of the Kerr Effect.

Taking the divergence of electric field, $\nabla^2 E$, and following the derivation in [3], we arrived at the expression below:

$$\frac{\partial A}{\partial z} = -\frac{1}{2}\beta_2 \frac{\partial^2 A}{\partial t^2} + i\gamma |A|^2 A - \frac{\alpha}{2} A$$

(3.41)

where α and γ is the fiber loss and nonlinear coefficient respectively, while β_2 is the group velocity dispersion (GVD) parameter. This equation is the Nonlinear Schrödinger Equation (NLSE) that

governs the envelope function of the optical pulse $A(z,t)$ under Kerr effect nonlinearity and loss in the optical fiber.

One of the common ways to solve NLSE in fiber optic is by using Split Step Fourier Method (SSFM). This computational method falls under the category of pseudo-spectral methods where the formula deals with all electromagnetic components without eliminating the carrier frequency [13]. In comparation with other NLSE solving methods, such as the time domain finite difference, SSFM is order of magnitude faster [14]. Although, SSFM is arguably less accurate because of the drop of the carrier frequency in the form of electric field and the inability to account for forward and backward propagating waves.

To proceed with the SSFM, Eq. (3.41) can be expressed as the combination of the linear operator, $\hat{L}$, and nonlinear operator, $\hat{N}$ as below:

$$\frac{\partial A(z,t)}{\partial z} = \left(\hat{L} + \hat{N}\right)A(z,t) \tag{3.42}$$

where

$$\hat{L} = -\frac{1}{2}\beta_2\frac{\partial^2}{\partial t^2} - \frac{\alpha}{2} \tag{3.43}$$

and

$$\hat{N} = i\gamma|A(z,t)|^2 \tag{3.44}$$

As the electric field envelope, $A(z,t)$ propagates from z to z+Δz, the analytical solution of Eq. (3.42) becomes:

$$A(\mathrm{z}+\Delta\mathrm{z},\mathrm{t}) = \exp\left(\Delta\mathrm{z}\left(\hat{L}+\hat{N}\right)\right)A(z,t) \tag{3.45}$$

assuming the two operators commute with each other, Eq. (2.45) then can be expressed as:

$$A(\mathrm{z}+\Delta\mathrm{z},\mathrm{t}) = \exp\left(\Delta z\hat{L}\right)\exp\left(\Delta z\hat{N}\right)A(z,t) \tag{3.46}$$

implying $A(\mathrm{z}+\Delta\mathrm{z},\mathrm{t})$ can be estimated by applying the two operators independently and the amount of Δz is sufficiently small. It has been reported that if the maximum phase shift, $\phi_{max} = \gamma\left|A_p\right|^2\Delta\mathrm{z}$, where A_p is the peak value of $A(z,t)$, is below 0.05 rad, SSFM gives a good result in most of contemporary optical communication systems [14].

To improve the computational time, symmetrized SSFM is introduced. In SSFM, the nonlinearity is assumed to be lumped at Δz, while in symmetrized SSFM, the nonlinearity is assumed to be distributed throughout Δz, results in:

$$A(\mathrm{z}+\Delta\mathrm{z},\mathrm{t}) = \exp\left(\frac{\Delta z}{2}\hat{L}\right)\exp\left(\frac{\Delta z}{2}\widehat{N}\right)A(z,t)\exp\left(\int_z^{z+\Delta z}\widehat{N}(z')dz'\right) \tag{3.47}$$

where

$$\int_z^{z+\Delta z}\widehat{N}(z')dz' \approx \frac{\Delta z}{2}[\widehat{N}(z)+\widehat{N}(z+\Delta z)] \tag{3.48}$$

for Δz that is sufficiently small.

However, iterative evaluation is needed due to the unknown value of $\widehat{N}(z+\Delta z)$ at $z+\frac{\Delta z}{2}$. The initial condition in this approach is by assuming $\widehat{N}(z+\Delta z)$ to be equal to $\widehat{N}(z)$. This iterative evaluation allows us the use larger Δz making improvement in terms of overall computational time.

3.2.3. Self-Phase Modulation (SPM)

SPM is the temporal analog to self-focusing that manifests as a narrowing spot size of CW beams in a nonlinear medium [3]. Some of the effects that are induced by SPM include nonlinear phase shifts and a change in pulse spectra.

3.2.3.1. Nonlinear Phase Shift

First, the normalized amplitude, $U(z,\tau)$, for the pulse propagation equation is introduced under the expression below:

$$A(z,t) = \sqrt{P_0}\exp\left(-\frac{\alpha z}{2}\right)U(z,\tau) \tag{3.49}$$

where τ is defined as:

$$\tau = \frac{T}{T_0} = \frac{t - z/v_g}{T_0} \tag{3.50}$$

where T is measured in a frame of reference with the pulse at the group velocity v_g and T_0 is the input pulse width. Depending on the input pulse width T_0 and the peak power P_0, dispersive or nonlinear effects may dominate along the fiber.

Putting the normalized amplitude, $U(z,\tau)$, into Eq. (3.32) in the limit β_2= 0, results in:

$$\frac{\partial U}{\partial z} = \frac{ie^{-az}}{L_{NL}}|U|^2U \tag{3.51}$$

where α accounts for fiber losses and the nonlinear length defined as:

$$L_{NL} = (\gamma P_0)^{-1} \tag{3.52}$$

Eq. (3.51) can be solved by introducing the $U = V\exp(i\varphi_{NL})$ and equating the real and imaginary parts so that:

$$\frac{\partial V}{\partial z} = 0;\ \frac{\partial \phi_{NL}}{\partial z} = \frac{e^{-az}}{L_{NL}}V^2 \tag{3.53}$$

As the amplitude V is constant along the fiber length L, the phase equation can then be integrated to obtain the general solution:

$$U(L,T) = U(0,T)\exp[i\phi_{NL}(L,T)] \tag{3.54}$$

where $U(0,T)$ is the field amplitude at $z = 0$ and the nonlinear phase expressed as:

$$\phi_{NL}(L,T) = |U(0,T)|^2\left(L_{eff}/L_{NL}\right) \tag{3.55}$$

and the effective length of the fiber is defined as:

$$L_{eff} = [1-\exp(-\alpha L)]/\alpha \tag{3.56}$$

Eq. (3.54) above shows that SPM gives rise to an intensity dependent phase shift while the pulse shape is maintained throughout the fiber. The maximum phase shift φ_{max} occurs at the pulse centered at $T = 0$. With U normalized such that $|U(0,0)|=1$, the maximum phase shift is defined as:

$$\phi_{max} = \frac{L_{eff}}{L_{NL}} = \gamma L_{eff} P_0 \tag{3.57}$$

A temporally varying phase implies that there is a variation of instantaneous optical frequency across the pulse from its central frequency ω_0. The frequency difference $\delta\omega$ is given by:

$$\delta\omega(T) = -\frac{\partial\phi_{NL}}{\partial T} = -\left(\frac{L_{eff}}{L_{NL}}\right)\frac{\partial}{\partial T}|U(0,T)|^2 \tag{3.58}$$

The time dependence of $\delta\omega$ is what we refer as frequency chirping that increases in magnitude as it propagates along the fiber. This phenomenon implies that new frequency components are

generated continuously during propagation and broaden the pulse spectrum. However, the qualitative features of frequency chirp depend on the pulse shape.

3.2.3.2. Changes in Pulse Spectra

The SPM-induced chirp can cause spectral broadening or narrowing depending on how the input pulse is chirped. For the unchirped input pulses, SPM will always lead to spectral broadening. An estimate of the magnitude of SPM-induced spectral broadening can be obtained from the peak value of $\delta\omega$ and calculate the peak value by maximizing $\delta\omega(T)$. The maximum value of $\delta\omega$ is given by setting its time derivative to zero:

$$\delta\omega_{max} = \frac{mf(m)}{T_0}\phi_{max} \tag{3.59}$$

where $f(m)$ is defined as:

$$f(m) = 2\left(1 - \frac{1}{2m}\right)^{1-1/2m} exp\left[-\left(1 - \frac{1}{2m}\right)\right] \tag{3.60}$$

To obtain the spectral broadening factor, the width parameter T_0 should be related to the initial spectral width $\Delta\omega_0$. For an unchirped Gaussian pulse, $\Delta\omega_0 = T_0^{-1}$, where $\Delta\omega_0$ is the 1/e half width. Eq. (2.59) for m=1 then becomes:

$$\delta\omega_{max} = 0.86\,\Delta\omega_0\phi_{max} \tag{3.61}$$

showing that the spectral broadening factor is approximately given by the maximum phase shift ϕ_{max}. SPM-induced spectral broadening is accompanied by an oscillatory structure on the entire frequency range as can be seen from to the time dependency of the frequency chirp where the amplitude and number of peaks depends on ϕ_{max}. The multipeak structure of the pulse is a result

of two waves of the same frequency that has different phases that interfere constructively or destructively depending on the relative phase difference.

3.2.4. Cross Phase Modulation (XPM)

When two or more optical waves co-propagate inside a fiber, they can interact with each other through fiber nonlinearity. The interaction can generate new waves under certain condition through variety of nonlinear phenomena. Coupling between incident waves also possible due to Cross-Phase Modulation (XPM) phenomena. XPM occurs due to the change of the effective refractive index as it depends of the intensity of that waves, as well as the intensity of the other copropagating waves.

3.2.4.1 Coupling Between Waves of Different Frequencies

One of the common XPM-induced effect on WDM is the coupling between waves of different frequencies. In the quasi-monochromatic approximation, separating the rapidly varying part of the electric field by writing it in the form:

$$\boldsymbol{E}(\boldsymbol{r},\boldsymbol{t}) = \frac{1}{2}\hat{x}\,[E_1 \exp(-i\omega_1 t) + E_2 \exp(-i\omega_2 t)] + c.c \tag{3.62}$$

where $\hat{x}$ is the polarization unit vector, ω_1 and ω_2 are the center frequencies of the two pulses with the corresponding amplitudes E_1 and E_2 are assumed to be slowly varying function of time.

The origin of XPM can be seen from the equation below:

$$\boldsymbol{P_{NL}}(r,t) = \tfrac{1}{2}\hat{x}\{P_{NL}(\omega_1)\exp(-i\omega_1 t) + P_{NL}(\omega_2)\exp(-i\omega_2 t) + P_{NL}(2\omega_1 - \omega_2)\ \exp[(-i(2\omega_1 - \omega_2)t] + P_{NL}(2\omega_2 - \omega_1)\exp[(-i(2\omega_2 - \omega_1)t] + c.c\} \tag{3.63}$$

The induced nonlinear polarization from the equation above shows that there are oscillating terms at the new frequencies $2\omega_1 - \omega_2$ and $2\omega_2 - \omega_1$ resulting from the phenomenon of Four Wave Mixing (FWM) while the remaining two terms provide the nonlinear contribution in the system.

As the waves propagates inside the fiber, the intensity-dependent nonlinear phase appears as:

$$\phi_j^{NL} = \frac{\omega_j z}{c}\Delta n_j = \frac{\omega_j z \bar{n}_2}{c}\left[\left|E_j\right|^2 + 2\left|E_{3-j}\right|^2\right] \tag{3.64}$$

where j=1 or 2. The first term contains the SPM term while the second contains the XPM term. The factor of 2 on the right side of equation shows that XPM is twice more effective for the same intensity.

3.2.4.2. Coupling Between Polarization Components of The Same Wave

The electric field associated with an elliptically polarized optical wave can be written in the form:

$$\boldsymbol{E}(\boldsymbol{r},\boldsymbol{t}) = \frac{1}{2}\left(\hat{x}E_x + \hat{y}E_y\right)\exp(-i\omega_0 t) + c.c \tag{3.65}$$

where $\hat{x}$ and $\hat{y}$ is the polarization unit vector, E_x and E_y are the complex amplitudes of the polarization components of the wave at central frequency ω_0. $\boldsymbol{P_{NL}}$ in an isotropic medium can be written as:

$$\boldsymbol{P_{NL}}(\boldsymbol{r},\boldsymbol{t}) = \frac{1}{2}\left(\hat{x}P_x + \hat{y}P_y\right)\exp(-i\omega_0 t) + c.c \tag{3.66}$$

The nonlinearity contribution Δn_x and Δn_y are given by:

$$\Delta n_x = \bar{n}_2 \left(|E_x|^2 + \frac{2}{3} |E_y|^2 \right) \tag{3.67}$$

$$\Delta n_y = \bar{n}_2 \left(|E_y|^2 + \frac{2}{3} |E_x|^2 \right) \tag{3.68}$$

The XPM between the two polarization components is less effective than the XPM between two different frequencies as can be seen from the factor of the second term that is smaller than the one in Eq. (3.64) although the qualitative behavior is the same. The XPM-induced nonlinear coupling between the field components create nonlinear birefringence that changes the polarization state of the elliptically polarized input light.

The slowly varying amplitudes A_x and A_y, defined by the expression below:

$$\frac{\partial A_x}{\partial z} + \beta_x \frac{\partial A_x}{\partial t} + \frac{i}{2} \beta_{2x} \frac{\partial^2 A_x}{\partial t^2} + \frac{\alpha}{2} A_2 = i\gamma \left(|A_x|^2 + \frac{2}{3} |A_y|^2 \right) A_x + \frac{i\gamma}{3} {A_x}^* {A_y}^2 \exp(-2i\Delta\beta z) \tag{3.69}$$

$$\frac{\partial A_y}{\partial z} + \beta_y \frac{\partial A_y}{\partial t} + \frac{i}{2} \beta_{2y} \frac{\partial^2 A_y}{\partial t^2} + \frac{\alpha}{2} A_2 = i\gamma \left(|A_y|^2 + \frac{2}{3} |A_x|^2 \right) A_y + \frac{i\gamma}{3} {A_y}^* {A_x}^2 \exp(-2i\Delta\beta z) \tag{3.70}$$

where the wavevector mismatch due to linear or model modal birefringence of the fiber is expressed as:

$$\Delta\beta = \beta_x - \beta_y \tag{3.71}$$

3.2.5. Four Wave Mixing (FWM)

FWM occurs due to the nonlinear response of bound electrons of the material and electromagnetic field. The polarization induced in this system is governed by the nonlinear susceptibility that has been previously mention in section 3.2.1. In general, FWM is polarization dependent. The third-order polarization term in the nonlinear relationship showing the main feature of the FWM as:

$$\boldsymbol{P_{NL}} = \epsilon_0 \chi^3 \vdots EEE \tag{3.72}$$

However, by considering the scalar case which all four fields are linearly polarized along the principal axis of birefringent such that the polarization is maintained along the transmission, we can get a physical insight on this effect. The total electric field of four linearly polarized along x-axis CW wavelengths that oscillating at frequencies ω_1, ω_2, ω_3, and ω_4 can be written as:

$$\boldsymbol{E} = \frac{1}{2}\hat{x}\sum_{j=1}^{4} E_j \exp\left[i(\beta_j z - \omega_j t\right] + c.c \tag{3.73}$$

If we substitute Eq. (3.72) to Eq. (3.73), and express $\boldsymbol{P_{NL}}$ the same way as $\boldsymbol{E}$ using

$$\boldsymbol{P_{NL}} = \frac{1}{2}\hat{x}\sum_{j=1}^{4} P_j \exp\left[i(\beta_j z - \omega_j t\right] + c.c \tag{3.74}$$

we find out that P_j consists of terms involving the products of the three electric fields,

$$\boldsymbol{P_4} = \frac{3\epsilon_0}{4}\chi^{(3)}_{XXXX}[|E_4|^2 E_4 + 2(|E_1|^2 + |E_2|^2 + |E_3|^2)E_4 + 2E_1E_2E_3\exp(i\theta_+) + 2E_1E_2E_3\exp(i\theta_-) + \cdots] \tag{3.75}$$

The first four terms containing E_4 are responsible for SPM and XPM while the remaining terms are the results of the four waves frequency combinations.

The scalar theory previously explained is based on the assumptions that all the optical fields are initially linearly polarized and maintain their State of Polarization (SOP) during propagation. In practice, the SOP of the signal is often arbitrary. However, FWM process is polarization dependent because the angular momenta among the four interacting photons should be conserved.

4. Gaussian Noise (GN) Model

GN model is based on the approximation that the nonlinear noise can be modelled as additive gaussian noise that is independent of ASE noise [5]. The idea is to have a simple mathematical model to inspect the nonlinearity of the transmission system, therefore avoiding complex computational methods to solve the NLSE in fiber optic transmission. The model takes advantage of the fact that long distance fiber transmission without group velocity dispersion compensation will disperse individual data bits over many bit periods. This effect results in nonlinear interactions between numerous data bits that can take on the characteristics of additive white Gaussian noise.

The power spectral density of this Gaussian nonlinear interference, G_{NLI}, itself is modeled as below:

$$G_{NLI}(f) = \frac{16}{27}\gamma^2 L_{eff}^2 \int_{-\infty}^{\infty}\int_{-\infty}^{\infty} G_{WDM}(f_1)\, G_{WDM}(f_2) G_{WDM}(f_1+f_2-f)\cdot \rho(f_1,f_2,f) \cdot \chi(f_1,f_2,f)\, df_2\, df_1 \tag{4.1}$$

where the G_{WDM} factors are the power spectral densities of the different WDM channels present in the system, including the channel of interest at frequency f. The lumped amplification factor (used for systems with EDFA amplification) is:

$$\rho(f_1,f_2,f) = \left|\frac{1-e^{-2\alpha L_s} e^{j4\pi^2\beta_2 L_s (f_1-f)(f_2-f)}}{2\alpha - j4\pi^2\beta_2 L_s (f_1-f)(f_2-f)}\right|^2 \cdot L_{eff}^{-2} \tag{4.2}$$

χ is known as the phased array factor, having the form of a phased array antenna, and accounts for the accumulation of the coherent interference at the receiver location at the end of the span:

$$\chi(f_1,f_2,f) = \frac{sin^2(2N_s\pi^2(f_1-f)(f_2-f)\beta_2 L_s)}{sin^2(2\pi^2(f_1-f)(f_2-f)\beta_2 L_s)}$$

(4.3)

In this equation, β_2 is the dispersion parameter, γ is the fiber non-linearity coefficient, L_s is the span length in km, α is the fiber loss coefficient, and N_s is the number of spans. L_{eff} is the effective length of the span given by: $\frac{1-\exp(-2\alpha L_S)}{2\alpha}$.

The equation above is known as the GN model Reference Formula (GNRF) that represents the power spectral density (PSD) of the NLI at the end of the link. The assumption is that every loss is exactly compensated by the optical amplifier gain and all of the spans that make up the link are identical.

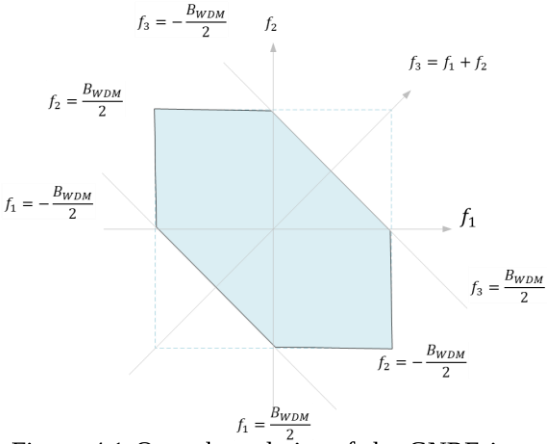

Figure 4.1 Outer boundaries of the GNRF integration domain to solve $G_{NLI}(f)$ at the center of the WDM spectrum (f=0) for Nyquist-WDM case.

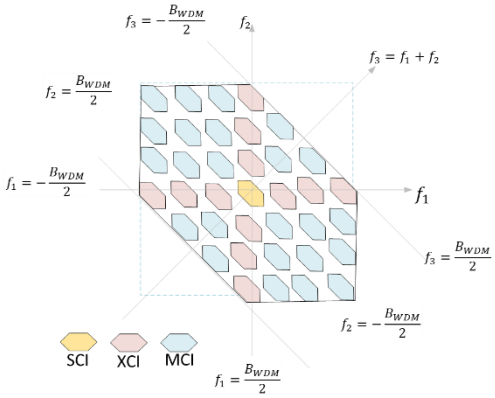

Figure 4.2 Outer boundaries of the GNRF integration domain to solve $G_{NLI}(f)$ at the center of the WDM spectrum (f=0) for B_{ch}= (2/3) Δf made up of 7 identical channels [15].

The expression in Eq. (4.1) shows that the process of the nonlinear interference (NLI) in the system follows a four-wave mixing (FWM)-like pattern where there are three frequency components, f_1, f_2, and $f_3 = (f_1 + f_2 - f)$ that contribute to the generation of the NLI noise at frequency f. The GNRF requires double integration over the WDM spectrum, determined by the WDM bandwidth B_{WDM}. The function can be referenced to a channel of interest at f=0. For a channel at the center of a band of WDM channels $G_{WDM}(f)=0$ for $f > B_{WDM}/2$ or $f < -B_{WDM}/2$. Detailed explanation on the GNRF integration domain is available in [15] and has contributions from the channel itself, SCI, neighboring channels, XCI, and a mixture of neighboring channels, MCI.

The PSD shape of the NLI, $G_{NLI}(f)$ is the main parameter to assess the system performance. If the $G_{NLI}(f)$ is approximately flat over the bandwidth for all transmission channels, the NLI will be considered as Gaussian and locally white.

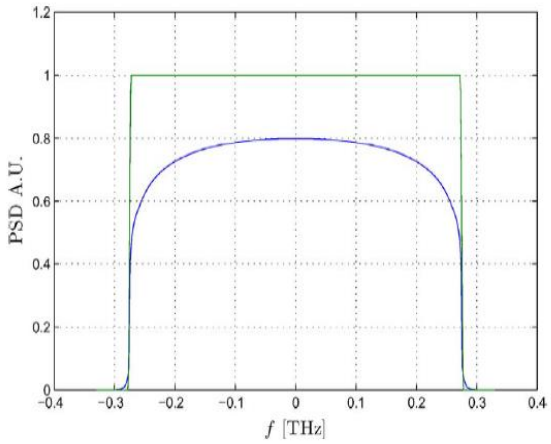

Figure 4.3. PSD of the transmitted signal GWDM(f) for 17 Nyquist-WDM channels at 32 Gbaud for 20 spans[15].

Many papers have looked intensively into the experimental validation of the 'Gaussianity' of the nonlinear noise in the transmission [15]. This underlying assumption is consistent with accumulated evidence [16] for systems with symbol rates $\geq$ 28 Gbaud, channel spacing up to 100 GHz, 3 channels minimum, over the fibers with D $\geq$ 2 ps/(nm.km).

Self-Channel Interference (SCI) is defined as pictured in Figure 4.2 where the 'island' sitting at the center contains all the three frequency components (f_1, f_2, f_3) beating at the center of the same channel, similar to self-phase modulation. Cross-Channel Interference (XCI) is similar to cross-phase modulation and defined as the contribution of the three frequency components generated from its own channel and one other channel. Multi-Channel Interference (MCI) defined as the contribution of the three frequency components generated from multiple different channels.

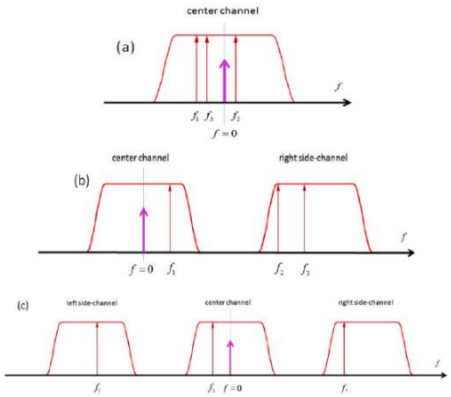

Figure 4.4. Purple short arrow: generated NLI. Red arrow: contributing signal components. (a) Self-Channel Interference (SCI); (b) Multi-Channel Interference (MCI); (c) Cross-Channel Interference (XCI) [15].

An approximation to solve the GNRF needs to be done for the performance assessment over a single span. For a Nyquist-WDM case, where the channel spectra are assumed to be perfectly rectangular with bandwidth equal to the symbol rate, with some approximation for this system, results in:

$$G_{NLI}(0) \approx \frac{8}{27}\gamma^2 G_{WDM}^3 L_{eff}^2 \frac{log_e\left(\frac{\pi^2}{2}\beta_2 L_{eff,a} B_{WDM}^2\right)}{\pi\beta_2 L_{eff,a}} \tag{4.4}$$

For large x, asinh $(x) \approx \log_e (2x)$ with a relative error less than 1% for $x = 3.5$. Using this approximation, the equation above becomes:

$$G_{NLI}(0) \approx \frac{8}{27}\gamma^2 G_{WDM}^3 L_{eff}^2 \frac{\text{asinh}\,(\pi^2 \beta_2 L_{eff,a} B_{WDM}^2)}{\pi \beta_2 L_{eff,a}} \tag{4.5}$$

where $L_{eff,a}$ is known as the asymptotic effective length defined as $1/2\alpha$. It should be noted that the span loss should be larger than 7 dB for this approximation to be accurate [15].

The G_{NLI} is used to calculate the NLI noise power for calculating the generalized Optical Signal-to-Noise-Ratio (gOSNR), given by:

$$gOSNR = \frac{P_{sig}}{P_{ASE} + P_{NLI}} \tag{4.6}$$

where P_{sig} is the average channel signal power, P_{ASE} is the ASE noise power, and P_{NLI} is the NLI noise power in the system. The correct formula for P_{NLI} is:

$$P_{NLI} = \frac{R_s}{B_H} \int_{-\infty}^{\infty} G_{NLI}(f + f_{ch}) |H_{RX}(f)|^2 df \tag{4.7}$$

where B_H is:

$$\int_{-\infty}^{\infty} |H_{RX}(f)|^2 df \tag{4.8}$$

$H_{RX}(f)$ is defined as the baseband scalar transfer function of the coherent receiver R_x. This equation requires a detailed knowledge of $H_{RX}(f)$ making it more complicated in the OSNR calculation. Although the GN model is not meant to calculate the OSNR of the system, by getting the $G_{NLI}(f_{ch})$ and assuming that the $G_{NLI}(f)$ is locally white across the channel bandwidth, the P_{NLI} then can be defined as:

$$P_{NLI} = G_{NLI}(f_{ch}) \cdot R_s \tag{4.9}$$

4.1 Coherent vs Incoherent GN Model

In the reference formula, G_{NLI} accounts for the coherent interference accumulated in a homogeneous and transparent link through the phase array factor, χ. An alternative model of the GN model that completely neglects coherent interference also known as Incoherent GN model (IGN) is introduced to further simplify the calculation of NLI.

As previously mentioned, when N_s>1, the phased array factor, χ, in the GNRF will have impact on the accumulation of the nonlinear noise along the link. The sum form of χ can be defined as below:

$$\chi(f_1, f_2, f) = N_s + 2\sum_{n=1}^{N_s-1}(N_s - n)\cdot cos(4n\pi^2)\,\beta_2 L_s(f_1 - f)(f_2 - f)) \tag{4.10}$$

Inserting this expression to the GNRF, the GNLI can be split into two expressions

$$G_{NLI}(f) = G_{NLI}^{inc}(f) + G_{NLI}^{cc}(f) \tag{4.11}$$

where the first term is purely incoherent noise accumulation defined as:

$$G_{NLI}^{inc}(f) = G_{NLI}(f)\cdot N_s \tag{4.12}$$

and the second term is the coherent coherence factor and can be considered small known as:

$$G_{NLI}^{cc}(f) = \frac{32}{27}\gamma^2 L_{eff}^2 \cdot \sum_{n=1}^{N_s-1}(N_s - n)\cdot \int_{-\infty}^{\infty}\int_{-\infty}^{\infty} G_{WDM}(f_1)\,G_{WDM}(f_2)G_{WDM}(f_1 + f_2 - f)\cdot \rho(f_1, f_2, f)\cdot cos\big(4n\pi^2|\beta_2|L_s(f_1 - f)(f_2 - f)\big)df_2\,df_1 \tag{4.13}$$

Following the derivation in [15], the two terms can be related by:

$$\epsilon = log_e\left(1 + \frac{G_{NLI}^{cc}(0)}{G_{NLI}^{inc}(0)}\right)\cdot\frac{1}{log_e(N_s)} \tag{4.14}$$

and the approximation formula of ϵ is defined as:

$$\epsilon \approx log_e\left(1+\frac{2L_{eff,a}\left[1-N_s+N_sHN\ (N_s-1)\right]}{N_sL_s\ asinh\left(\frac{\pi^2}{2}\beta_2 L_{eff,a}B_{WDM}^2\right)}\right)\cdot\frac{1}{log_e(N_s)} \tag{4.15}$$

where HN is the Harmonic Number that depends on the modulation format.

Therefore, for a homogeneous Non-Nyquist-WDM link the closed form formula would be the following:

$$G_{NLI}(0) \approx \frac{8}{27}\frac{\gamma^2 G_{WDM}^3 L_{eff}^2}{\pi\beta_2 L_{eff,a}}\ \text{asinh}\left(\frac{\pi^2}{2}\beta_2 L_{eff,a}B_{ch}^2 N_{ch}^{2\frac{B_{ch}}{\Delta f}}\right)\cdot N_s^{1+\varepsilon} \tag{4.16}$$

If $B_{ch} = \Delta f$:

$$B_{ch}^2 N_{ch}^{2\frac{B_{ch}}{\Delta f}} = B_{WDM}^2 \tag{4.17}$$

then the equation to the Nyquist WDM case is found. Due to the nature of the approximation, it is worth noting that this equation is accurate for the following system parameters: span loss $\geq$ 7 dB, $\beta_2 \geq 4$, $R_s \geq$ 28 Gbaud, and $B_{ch}/\Delta f \geq 0.25$ [15]. In this equation, having $\epsilon = 0$ means that the NLI produced in the span sums up incoherently (IGN Model)

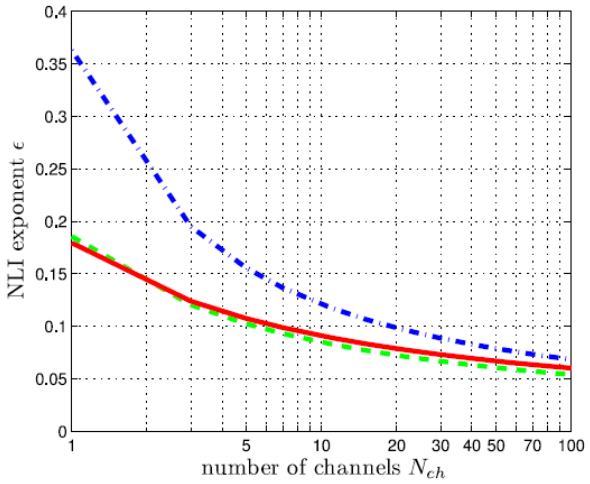

Figure 4.5. ϵ factor versus number of channels in a 32 Gbaud, 50 GHz channel spacing, with a 100 span length system, tested over 3 types of fiber. Red solid line: PSCF; green dashed line: SMF; blue dash-dotted line: NZDSF [5].

It can be seen that ϵ is relatively small and exponentially decreases as the number of channels is increased. Various experimental results [19], [20], [21] show that ϵ is essentially linear with the number of spans with very slight impact in the noise accumulation in the original GN model.

4.2. GN Model Revised Version

The simplicity of GN-model for calculating the nonlinear effect in fiber transmission has triggered the development of the research of using this approach on DM transmission. Perturbative models so far have not worked well in DM type transmission [15]. In transmission where the signal is not dispersed enough, it requires a more complex solution to solve the highly phase-dependent characteristics of nonlinear noise, such as the SSFM method.

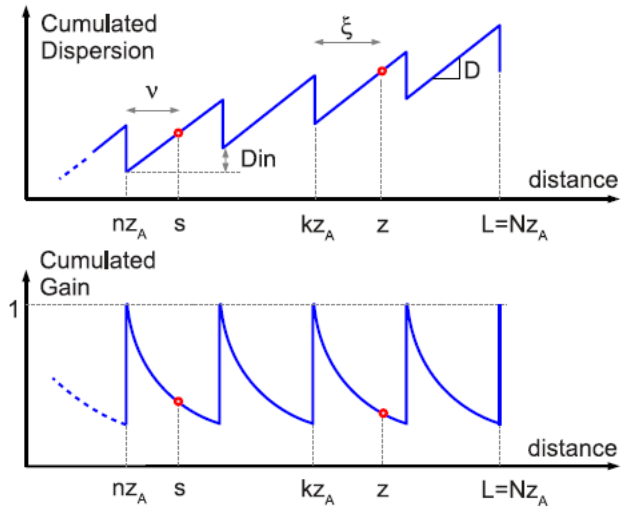

Figure 4.6. Dispersion Map of a DMT Homogeneous Link [17].

To deal with this characteristic, a Pre-Dispersion compensation mechanism (PD) can be applied at the transmitter side and it is shown that the nonlinear prediction is matched to that of the UT link calculated using the GN-model [18].

Some other attempts to increase the accuracy of this prediction have also been done by modifying the integration domain [18], [19], to account for the over-estimated value due to the weak Gaussianity assumption. The revision over the closed-form solution of the GN-model for a PD-DM system is shown in [18] as:

$$G_{NLI}(0) \approx \frac{8}{27}\frac{\gamma^2 G_{WDM}^3 L_{eff}^2}{\pi\beta_2 L_{eff,a}} \operatorname{asinh}\left(\frac{3\pi}{8}\beta_2 L_{eff,a} B_{ch}^2 N_{ch}^{2\frac{B_{ch}}{\Delta f}}\right) \cdot N_s^{1+\varepsilon_{revised}} \tag{4.18}$$

With the $\varepsilon_{revised}$ is defined as:

$$\varepsilon_{revised} \approx \frac{3}{10} log_e\left(1 + \frac{6}{\sqrt[3/4]{(1-d)L_s}} \cdot \frac{L_{eff,a}}{\operatorname{asinh}\left(\frac{3\pi}{8}\beta_2 L_{eff,a} B_{ch}^2 N_{ch}^{2\frac{B_{ch}}{\Delta f}}\right)}\right) \tag{4.19}$$

where d is the dispersion compensation ratio.

4.3. QoT Prediction Model

Flexible and dynamic operation of future networks will require the signal transmission performance to be predicted before a certain wavelength, modulation method, or any other network parameter is assigned. In the recent years, researchers have been developing methods to predict the QoT using several prediction models, most notably, using Machine Learning (ML) for SDN-controlled network [8], [9].

One optical fiber transmission tool that was recently released from the initiative of the network engineering community founded in 2016, known as the Telecom Infra Project, Inc (TIP). The Open-Optical Packet-Transport (OOPT) Group within TIP have been working on a large-scale transmission modelling tool, the Optical Link Emulator (OLE), and it has been tested on multiple testbeds provided by the industry, such as Microsoft and Facebook [22].

While ML predicts the network behavior by taking multiple inputs and data from the system, the OLE uses the GN model calculation to be able predict the QoT of the system. This model has been developed in Python and is commonly known as the GNPy tool. The results of experimental validation on long haul transmission systems also has shown good agreement with simulation [22]. This reasonable accuracy and the simplicity of the GN-model becomes a powerful feature to be implemented in a latency-sensitive network.

GNPy utilizes the IGN model as it is proven to have good accuracy while offering more simplicity in the calculation process. All the design and network parameters are defined in JSON , a light, open-standard data-interchange format file. The designs included in the library are ROADMs, EDFAs, transceivers, and transmission link parameters.

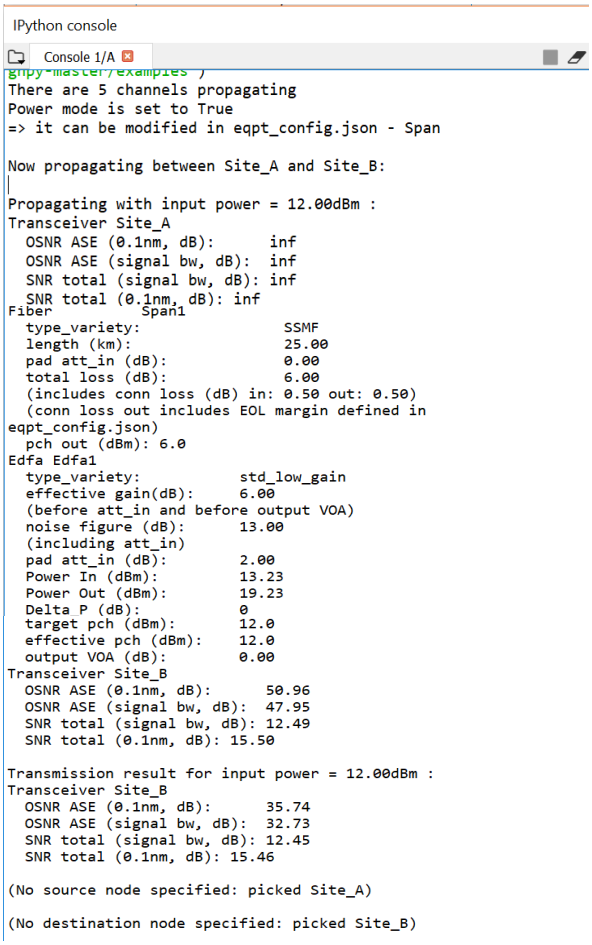

Figure 4.7. Output sample of gnpy for 5 channels transmitted over a 25 km span.

From the figure above, we can see the SNR predicted by gnpy for single span transmission with 5 channels. This result will later be compared to the experimental results that was done for this thesis in the experimental section.

5. Experiments

5.1 Transmission Setup

In this system, CW light with wavelength λ=1555.243 nm from the Integrated Tunable Laser (ITLA) was connected to an 40 GHz IQ Modulator. A signal generator is also connected to the modulator, feeding it with 25 Gbps bitrate NRZ data with a 2^{11}-1 PRBS bit sequence. The signal coming out of the modulator was then split with the signal in one arm delayed to decorrelate the signal creating a dual polarization system. The polarization controller at both arms control each arm's polarization before the signal was combined by a Polarization Beam Combiner (PBC).

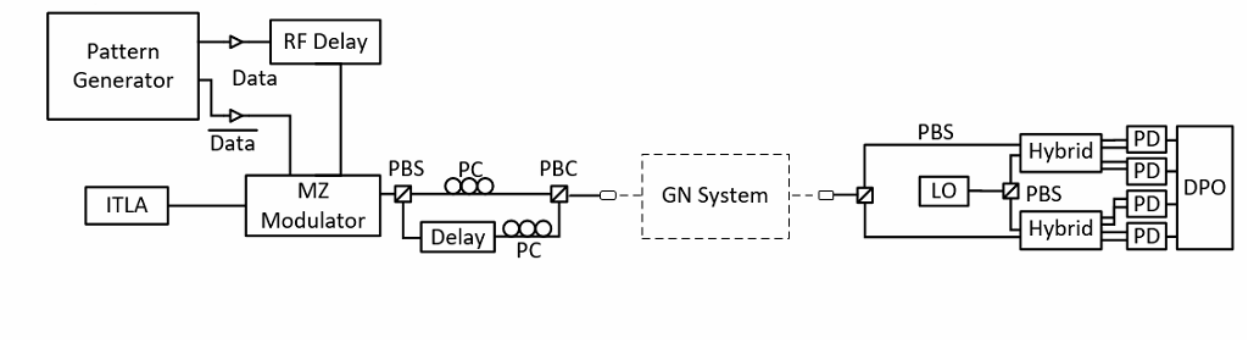

Figure 5.1. Optical coherent transmitter and receiver configuration

A broadband ASE source with C-band range acted as the interference channels with the bandwidth equal to 25 GHz per channel. This signal shaping was done by connecting the broadband ASE source to a Wavelength Selective Switch (WSS) that was set to the desired bandwidth resulting a 5 channel transmission system as can be seen below. This signal was then combined with the signal coming out of the coherent transmitter using a 3dB coupler.

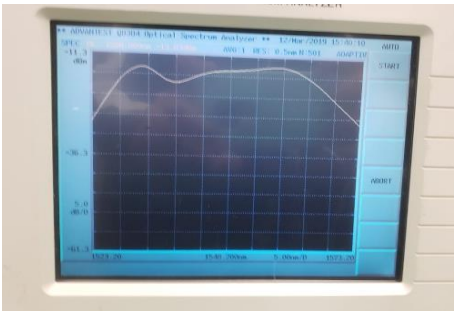

Figure 5.2. Spectrum of the broadband laser

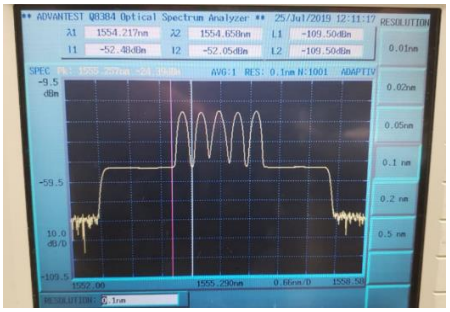

Figure 5.3. Five transmitted channels with equal bandwidth

The combined signal at the output of the coherent transmitter then went into a 25 km fiber span consisting of standard single mode fiber SMF and the power was controlled by a Variable Optical Attenuator (VOA). Amplification was needed to obtain high signal power, up to +10 dBm. Therefore, to achieve such power levels, three EDFAs were used. One EDFA was used to amplify the signal coming from the broadband laser while two EDFAs were used to amplify both signals coming from the ITLA and broadband ASE source that was combined by a 3dB coupler. To monitor the signal that went into the span, a 1x2 splitter with splitting ratio of 1:99 was used. This splitter sends 1% of the signal into an internal power monitoring feature of the WSS called the Optical Channel Monitor (OCM) and transmits the rest of the signal into the span. To calibrate the splitters used in this system, the splitting ratio of these splitters were measured by checking the output power at each port using an Optical Power Meter (OPM).

Figure 5.4. Optical Channel Monitor (OCM) feature of WSS

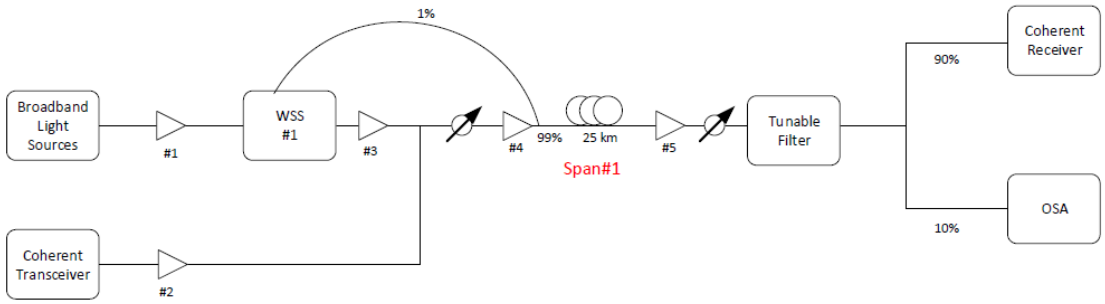

Figure 5.5. GN Model Experiment Setup for 1 Span

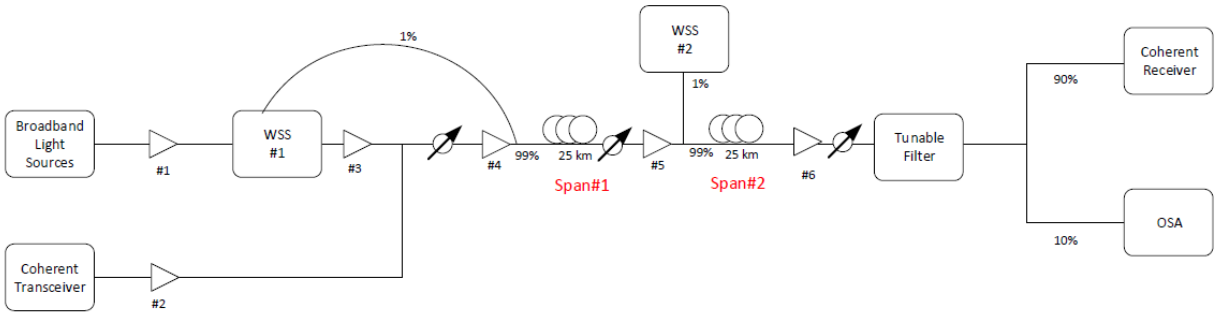

Figure 5.6. GN Model Experiment Setup for 2 Spans

The link consists of either one or two spans where the second span consists of an equal span length and the same fiber type (homogeneous) with another VOA to control the signal power that is launched into the second span (transparent). At the end of each span, an EDFA was used to compensate for the fiber loss. The receiver end consists of four balanced photo-detectors with internal Trans Impedance Amplifiers (TIA) to amplify the signal that goes into the real-time sampling oscilloscope called digital phosphor oscilloscope (DPO) after passing a tunable filter to eliminate out of band noise and signal power. At the DPO, offline digital signal processing (DSP)

is used to process the detected signal and calculate the received BER with the pattern length BER limit of 2.5 x 10^{-5}.

5.2. Back-to-Back (B2B) Measurement

Initial measurements were performed consisting of back to back (B2B) performance and the performance after one or two transmission spans. To characterize the BER and OSNR relation of the system, the ASE noise power, $P_{ASE,}$ modeled as:

$$P_{ASE} = nF(G-1)hvB_n \tag{5.1}$$

and the OSNR measured at the end of the link is equal to:

$$OSNR = \frac{P_{in}}{nF(G-1)hvB_n} \tag{5.2}$$

Here n is the number of amplifiers, F is the amplifier noise factor, G is the gain of the amplifier, h is the Plank's constant, v is the center frequency of the channel, and B_n is the noise reference bandwidth which was set to 0.1 nm, 12.5 GHz.

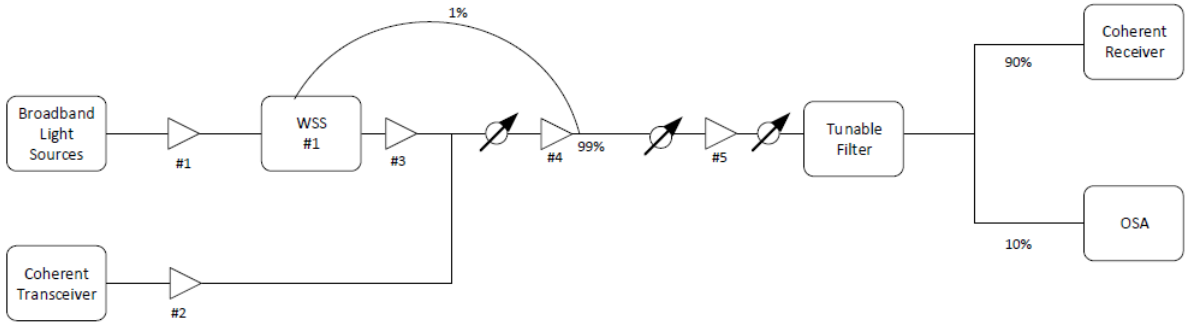

Figure 5.7. B2B Measurement Setup

In the ideal system where there is only Gaussian optical noise and assuming a receiver that has a matching transfer function to the transmitted symbols, the BER for PM-QPSK modulation is given by [16]:

$$BER = \frac{1}{2} erfc\left(\sqrt{gOSNR \frac{B_n}{2R_s}}\right) \tag{5.3}$$

It should be noted that in B2B measurement, $gOSNR$ in the equation above is due to ASE noise only, which is Gaussian. In the actual system, various transmitters and receivers suffer non-ideal characteristics, therefore the BER vs OSNR dependency should be calibrated by inserting a factor *k* into the BER equation above results in:

$$BER = \frac{1}{2} erfc\left(\sqrt{k.gOSNR \frac{B_n}{2R_s}}\right) \tag{5.4}$$

The OSNR was measured using an optical spectrum analyzer, OSA, with the out-of-band measurement method, which involves measuring the noise power adjacent to the signal and extrapolating to get the noise power within the channel. The B2B test here was performed without noise loading, but instead performed by varying the signal power into the amplifiers to vary the OSNR. The BER was also measured using the DPO and converted to the corresponding OSNR using Eq (5.3). Both of these results were combined in the figure below.

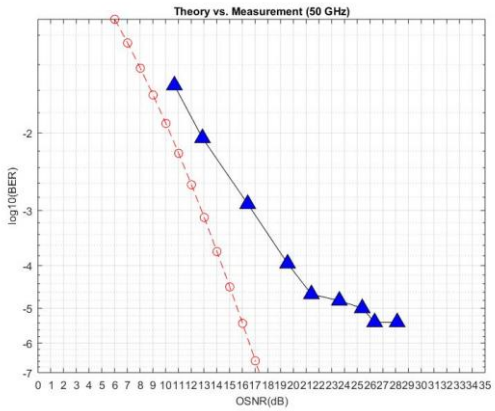

Figure 5.8. OSNR vs BER curve

In the figure above, the OSNR show a relatively close fit to the theoretical curve with the error floor at around 26 dB OSNR. To fit the OSNR measured by the OSA to the theoretical curve of the BER, the k factor in Eq (5.4) should be multiplied with the OSNR. To obtain this k factor, the ideal OSNR converted from the BER should be divided by the OSNR measured by the OSA resulting in the OSNR dependent k factor shown in the figure below. This k factor later was used to convert the measured gOSNR in all experiments.

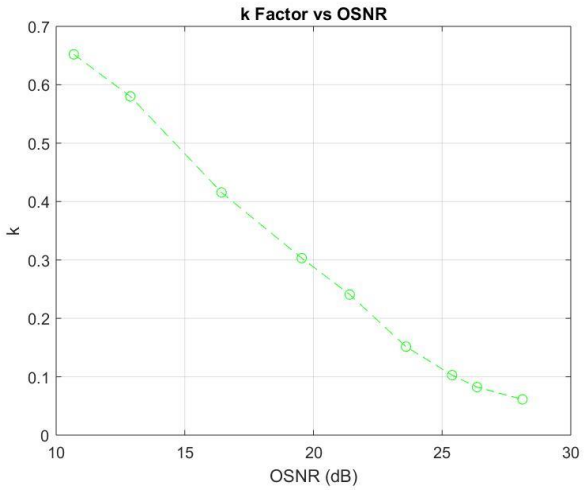

Figure 5.9. Calculated k factor

The OSNR measurement was done using the OSA at 0.2 nm resolution for the signal power and 0.1 nm resolution for the noise power, therefore the OSNR was measured as:

$$OSNR = \frac{P_{sig} - P_{ASE} \cdot 2}{P_{ASE}} \tag{5.5}$$

Since there was a VOA and filter before the OSA, the power measured at the OSA was the scaled down level after being attenuated. Therefore, a simple calculation needed to be performed to scale up and get the actual ASE power level to be put inside the gOSNR formula.

In these experiments the signal power into the receiver was kept constant and also the OSNR at the receiver for a given signal power was adjusted to be the same for the 1 span and 2 spans measurements. In this way the difference between the 1 span and 2 spans result for the gOSNR will be due to the nonlinear noise only.

5.3 Measurement Results

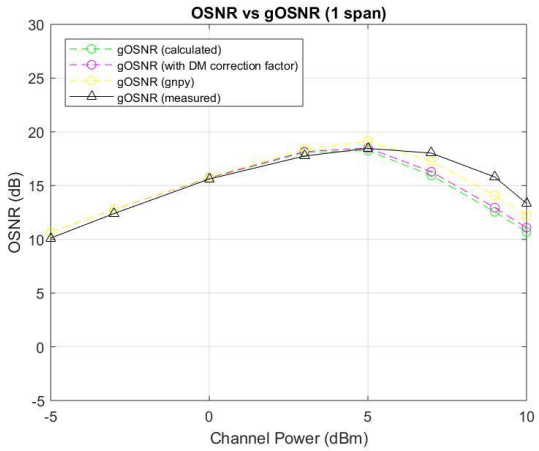

Figure. 5.10. gOSNR comparison for 1 span. Green: calculated using GN Model; Purple: calculated using GN for DMT; Yellow: results from gnpy; Black: experimental result

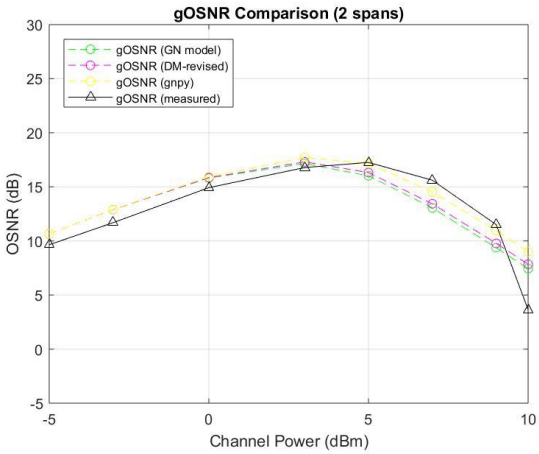

Figure. 5.11. gOSNR comparison for 2 spans. Green: calculated using GN Model; Purple: calculated using GN for DMT; Yellow: results from gnpy; Black: experimental result

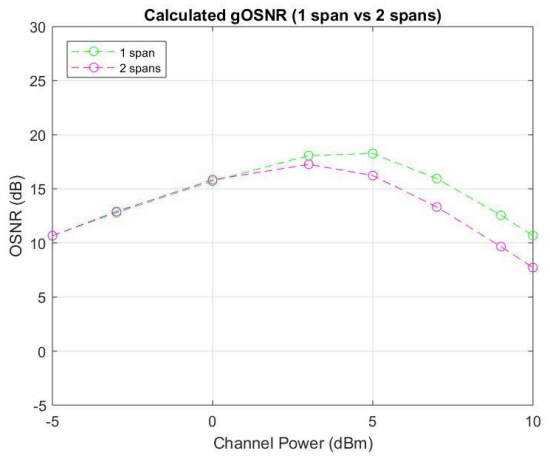

Figure. 5.12. 1 span vs 2 spans gOSNR comparison calculated using GN Model

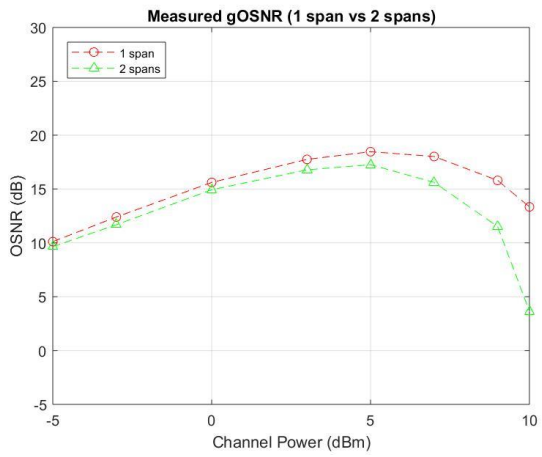

Figure 5.13. Experimental results of gOSNR for 1 span vs 2 spans

As the results show, the gOSNR measured shows reasonable agreement, although the calculated nonlinear impact is larger. It was shown in published simulation studies that the GN model overestimates the NLI power of the first few spans where the signal is farther from a Gaussian distribution and only moderately dispersed [23]. The calculated gOSNRs at high power are consistent below the measured, except for the 2 span, 10 dBm signal power case, although the signal is so strongly impaired by nonlinear effects that the BER estimation accuracy is likely a factor here. Comparing the 1 and two span case, both the calculated and measured results show an earlier onset of nonlinear impact, but the calculated case is slightly more pronounced. The 2 span case nevertheless more closely agrees with the calculation. There is also a slight difference between the simulation done for this thesis compared to the result from gnpy, where the IGN model was used here and GNPy uses an enhanced closed form version of the IGN model.

The Enhanced Gaussian Noise (EGN) Model relaxes the Gaussianity assumption from the NLI noise [4]. However, the additional complexity of this model increases the computational process in the QoT prediction of the system. Therefore, in [23], a correction term to accommodate for this inaccuracy is defined as:

$$G_{corr} = \frac{80}{81}\Phi\frac{\gamma^2\bar{L}_{eff}^2 P_{ch}^3 N_s}{R_s^2\Delta f\pi\beta_2\bar{L}_s}HN(\frac{[N_{ch}-1]}{2})$$

(5.7)

where G_{corr} is the closed-form correction term, $\bar{L}_s$ is the average span length (km), and $\bar{L}_{eff}$ is the average effective length. HN(N) is the new term added using the harmonic number series as:

$$HN(N) = \sum_{n=1}^{N}\frac{1}{n}$$

(5.8)

Finally, Φ is a constant that depends on the modulation format, with the values: 1 for PM-QPSK, 17/25 for PM-16QAM and 13/21 for PM-64QAM. In these results, the correction factor turns out to be negligible. The results of this experiment shown that there was a significant deviation of the measured gOSNR penalty for the short span transmission compared to calculations. The correction term used in the calculation also did not show any significant improvement to the accuracy. This is possibly due to the failing Gaussianity assumption that has been addressed in many papers [16]. To further analyze the results, we recorded the constellation points of the received signals at high power.

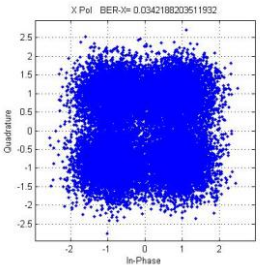

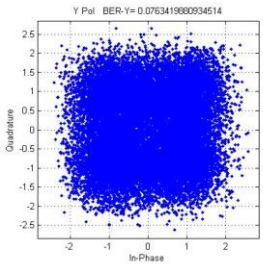

Figure 5.14. Constellation point at the receiver for X polarization (left) and Y polarization (right) and P_{Tx} = -5 dBm after 1 span

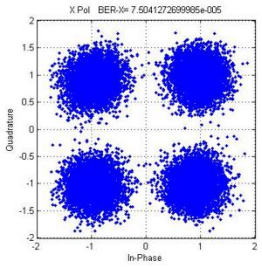

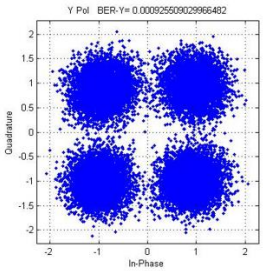

Figure 5.15. Constellation point at the receiver for X polarization (left) and Y polarization (right) and P_{Tx} = 3 dBm after 1 span

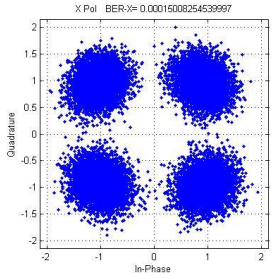

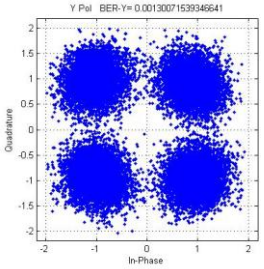

Figure 5.16. Constellation point at the receiver for X polarization (left) and Y polarization (right) and P_{Tx} = 7 dBm after 1 span

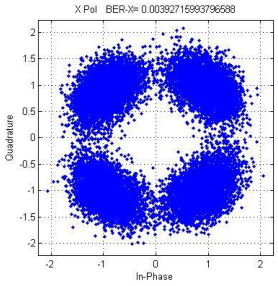

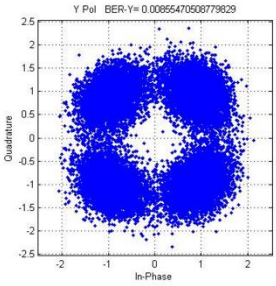

Figure 5.17. Constellation point at the receiver for X polarization (left) and Y polarization (right) and P_{Tx} = 10 dBm after 1 span

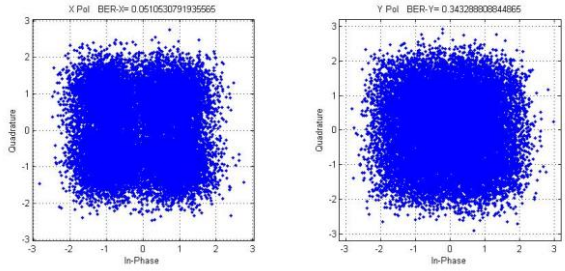

Figure 5.18. Constellation point at the receiver for X polarization (left) and Y polarization (right) and P_{Tx} = -5 dBm after 2 spans

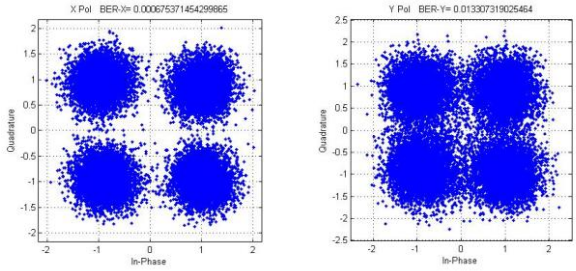

Figure 5.19. Constellation point at the receiver for X polarization (left) and Y polarization (right) and P_{Tx} = 3 dBm after 2 spans

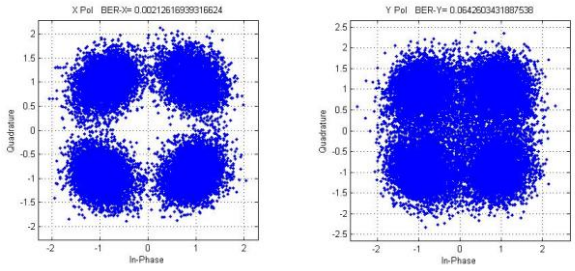

Figure 5.20. Constellation point at the receiver for X polarization (left) and Y polarization (right) and P_{Tx} = 7 dBm after 2 spans

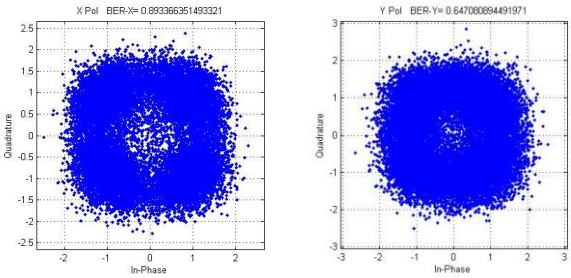

Figure 5.21. Constellation point at the receiver for X polarization (left) and Y polarization (right) and P_{Tx} = 10 dBm after 2 spans

From the image above, it can be seen that at the higher power (7 dBm and 10 dBm), the constellation point no longer show the circular Gaussian shape and are distorted due to the high nonlinear phase noise effect.

5.4 Dispersion Analysis

For the received signal distribution to be considered Gaussian or following the condition of the GN model, the system needs to be highly dispersed [17]. In this experiment for 1 short span, it is showing a different result from what the model predicted. This phenomenon is possibly due to the low group velocity dispersion occurring in the system. Using the dispersion parameter, *D*, equal to 16.7 ps/nm.km, signal bandwidth of 0.2 nm corresponding to a 40 ps bit duration, and the

span length of 25 km, the dispersion group delay can be simply estimated resulting in < 83.5 ps group delay within the signal band. This corresponds to 2.08 times bit period. For 50 km, the signal will be dispersed more to 167 ps or equal to 4.17 times initial bit period. This means that at worst nearest neighbors (1 span) or next nearest neighbor bits (2 spans) will interact with each other, far from the highly dispersed case assumed in the Gaussian noise model.

5.5. Power vs Nonlinear Effect

In addition to understanding the short span case, this work seeks to explore the potential for using a few short spans to emulate longer distance (more span hops) transmission. As been derived in [24], P_{NLI} essentially can be written as:

$$P_{NLI} = \eta_{NLI}\gamma^2 \cdot N_{span} \cdot {P_{Tx,ch}}^3 \tag{5.14}$$

Where $\eta_{NLI}\gamma^2$ is the 'nonlinear lever' that is used to compare the nonlinear strength of different fiber types. However, in this experiment, to produce a high nonlinear noise equal to that of multiple spans, the power at the transmitter was increased. By a simple calculation, it can be concluded that the power of the signal should be increased by a factor of $(N_{span})^{1/3}$ launching into one span to achieve an effect similar to what would be seen after N-th span. Therefore, $P_{NLI}\left(P_{Tx,ch}, N_{span}\right) = P_{NLI}(P^*, 1)$, where $P* = (N_{span})^{1/3} \cdot P_{Tx,ch,1sp}$. The distance dependence of the P_{NLI} is shown in Figure 5.22. In the figure, for example, we can see how the P_{NLI} for 30 spans at -5 dBm can be achieved by launching 0 dBm to 1 span. Thus, using the measured P_{NLI} versus the launch power for 1 span $P_{Tx,ch,1sp}$, the P_{NLI} after N_{spans} can be found by multiplying the launch power by the cube-root of the number of spans and plugging this power into the measured 1 span P_{NLI} versus launch power curve.

In Figure 5.23, the gOSNR of multiple spans are simulated based on the calculated PNLI of 1 span. Gnpy is also used to simulate this effect. To get the similar gOSNR number with the simulation result, the amplifiers are set at a constant gain of 18 dB. To calculate for the nonlinear accumulation of the multiple spans, ε factor of 0.1 is used in the model as the correction factor. In the figure we can see that the gOSNR plot shifts as the number of spans increase.

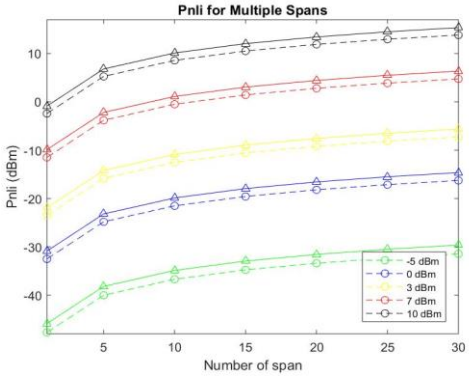

igure 5.22 P_{NLI} over multiple number of spans for various transmitted channel power. Solid line: P_{NLI} from gnpy. Dashed line: P_{NLI} calculated from GN model

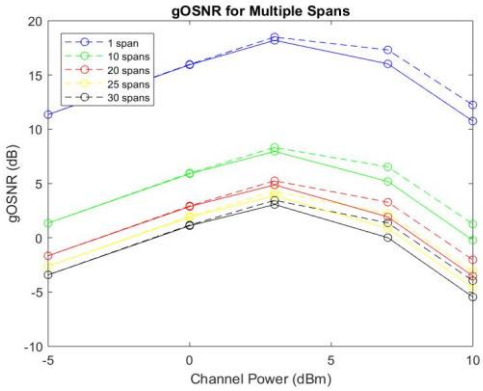

Figure 5.23 $gOSNR$ over multiple number of spans for various transmitted channel power. Solid line: $gOSNR$ from gnpy. Dashed line: $gOSNR$ calculated from GN model

It is important to note that much additional measurement and characterization is needed in order to confirm the effects shown here and to establish both the short span behavior and the correction factor going from a single span measurement to multiple spans. In particular, the multi-span case used the GN model calculations as a reference, but actual measured results are still needed. However, the GN model calculations are expected to be a good reference as they have been evaluated in many studies to show good agreement after long transmission distances. It will also be important to separate the effects of a short span length as well as looking at even shorter spans, going down to just a few kilometers, as might be expected in urban environments.

6. Conclusion

Nonlinear signal impairments are among the most critical impairments in long-haul optical fiber transmission. The attempt to predict this effect has led researchers to come up with many nonlinear prediction models to be implemented in Quality of Transmission (QoT) prediction algorithms, such as the GN model. In uncompensated transmission systems, the GN model has been proven to provide accurate prediction in long-haul WDM systems. However, in metro networks where the transmission link consists of short spans with different types of fiber, the performance of GN model should be inspected.

In this thesis, the performance of the GN model was tested in one and two short span transmission consisting of 25 km fiber in each span. In this experiment, the GN model shows reasonable accuracy for both cases with maximum deviation of + 3 dB at high levels of nonlinear distortion. The low levels of chromatic dispersion may have contributed to this deviation as the group delay is less than 4.17 times initial bit period in this case. The distortion in the constellations is shown by the curvature in the constellation points due to nonlinear phase shifts.

The effect of nonlinear noise over multiple spans for multiple channel power is also inspected in this thesis. This will be essential to simulate the nonlinear impact of many hops by increasing the power launched into the system. The power of the signal should be increased by a factor of $(N_{span})13/$ launching into one span to achieve an effect similar to what would be seen after N_{span}. However, this should be tested further in future experiments considering the phase-dependent nature of the nonlinear noise.

The main contribution of this thesis has been an initial study of the application of the GN model to estimating performance of transmission over short spans. This short span transmission is 60

common in urban areas (e.g. Metro networks), but also by exploiting the power and span dependency of nonlinear noise power, we emulate the multi-hop transmission nonlinear effect using a single span. This will be beneficial in lab setups in which setting up a recirculating loop or deploying a large-scale system is not an option.

References

[1] Kilper, D.C, et al. “Power Trends in Communication Networks.” *IEEE Journal of Selected Topics in Quantum Electronics*, vol. 17, no. 2, 2011, pp. 275–284., doi:10.1109/jstqe.2010.2074187.

[2] Xu, Kaikai, and Yang Ou. "Theoretical and numerical characterization of a 40 Gbps long-haul multi-channel transmission system with dispersion compensation." *Digital Communications and Networks* 1.3 (2015): 222-228.

[3] Govind P. Agrawal. “Nonlinear Fiber Optics”. 2013

[4] Carena, Andrea, et al. "EGN model of non-linear fiber propagation." *Optics express* 22.13 (2014): 16335-16362.

[5] Poggiolini, Pierluigi, et al. "The GN-model of fiber non-linear propagation and its applications." *Journal of lightwave technology* 32.4 (2013): 694-721.

[6] P. Serena and A. Bononi, “On the accuracy of the gaussian nonlinear model for dispersion-unmanaged coherent links,” presented at the Eur.Conf. Opt. Commun., London, U.K., Sep. 2013, Paper Th.1.D.3.

[7] Sartzetakis, I., et al. "Quality of transmission estimation in WDM and elastic optical networks accounting for space–spectrum dependencies." IEEE/OSA Journal of Optical Communications and Networking 8.9 (2016): 676-688.

[8] Yan, Shuangyi, et al. "Field trial of machine-learning-assisted and SDN-based optical network planning with network-scale monitoring database." 2017 European Conference on Optical Communication (ECOC). IEEE, 2017.

[9] Mo, Weiyang, et al. "ANN-based transfer learning for QoT prediction in real-time mixed line-rate systems." 2018 Optical Fiber Communications Conference and Exposition (OFC). IEEE, 2018.

[10] Auge, Jean-Luc, et al. "Open optical network planning demonstration." Optical Fiber Communication Conference. Optical Society of America, 2019.

[11] K. Kikuchi, "Fundamentals of Coherent Optical Fiber Communications," in Journal of Lightwave Technology, vol. 34, no. 1, pp. 157-179, 1 Jan.1, 2016.

[12] Jacobs, Stephen (30 November 1962). Technical Note on Heterodyne Detection in Optical Communications (Report). Syosset, New York: Technical Research Group, Inc. Retrieved 15 February 2017.

[13] Suarez, Pablo. (2015). An introduction to the Split Step Fourier Method using MATLAB. 10.13140/RG.2.1.1394.0965.

[14] Lee, Jong-Hyung. Analysis and characterization of fiber nonlinearities with deterministic and stochastic signal sources. Diss. Virginia Tech, 2000.

[15] Poggiolini, Pierluigi. "The GN model of non-linear propagation in uncompensated coherent optical systems." Journal of Lightwave Technology 30.24 (2012): 3857-3879.

[16] Johannisson, Pontus, and Erik Agrell. "Modeling of nonlinear signal distortion in fiber-optic networks." Journal of Lightwave Technology 32.23 (2014): 4544-4552.

[17] Serena, Paolo, and Alberto Bononi. "An alternative approach to the Gaussian noise model and its system implications." Journal of Lightwave Technology 31.22 (2013): 3489-3499.

[18] Qiao, Yaojun, et al. "Analytical expressions for the nonlinear interference in dispersion managed transmission coherent optical systems." Optics Communications 335 (2015): 116-125.

[19] Savory, Seb J. "Approximations for the nonlinear self-channel interference of channels with rectangular spectra." IEEE Photonics Technology Letters 25.10 (2013): 961-964.

[20] F. Vacondio, C. Simonneau, L. Lorcy, J. C. Antona, A. Bononi, and S. Bigo, “Experimental characterization of Gaussian-distributed nonlinear distortions,” presented at the Eur. Conf. Opt. Commun., Geneva, Switzerland, paper We.7.B.1, Sep. 2011.

[21] G. Bosco, R. Cigliutti, A. Nespola, A. Carena, V. Curri, F. Forghieri, Y. Yamamoto, T. Sasaki, Y. Jiang, and P. Poggiolini, “Experimental investigation of nonlinear interference accumulation in uncompensated links,” IEEE Photon. Technol. Lett., vol. 24, no. 14, pp. 1230–1232, Nov. 15, 2012.

[22] Grammel, Gert, Vittorio Curri, and Jean-Luc Auge. "Physical simulation environment of the telecommunications infrastructure project (TIP)." Optical Fiber Communication Conference. Optical Society of America, 2018.

[23] Poggiolini, Pierluigi, et al. "A simple and effective closed-form GN model correction formula accounting for signal non-Gaussian distribution." Journal of Lightwave Technology 33.2 (2015): 459-473.

[24] G. Bosco, A. Carena, R. Cigliutti, V. Curri, P. Poggiolini, and F. Forghieri, “Performance prediction for WDM PM-QPSK transmission over uncompensated links,” in Optical Fiber

Communication Conference, OSA Technical Digest (CD) (Optical Society of America, 2011), paper OThO7.

[25] Mo, Weiyang, et al. "Deep-neural-network-based wavelength selection and switching in ROADM systems." Journal of optical communications and networking 10.10 (2018): D1-D11.